8-23-2013

Impact of MHD Shock Physics on Magnetosheath Symmetry and Kelvin-Helmholtz Instability

K. Nykyri
Embry-Riddle Aeronautical University, nykyrik@erau.edu

Scholarly Commons Citation

Nykyri, K. (2013), Impact of MHD shock physics on magnetosheath asymmetry and Kelvin-Helmholtz instability, J. Geophys. Res. Space Physics, 118, 5068–5081, doi:10.1002/jgra.50499

Impact of MHD shock physics on magnetosheath asymmetry and Kelvin-Helmholtz instability

K. Nykyri[1]

Received 29 March 2013; revised 31 July 2013; accepted 5 August 2013; published 23 August 2013.

[1] We have performed 13 three-dimensional global magnetohydrodynamic (MHD) simulations of the magnetosheath plasma and magnetic field properties for Parker spiral (PS) and ortho-Parker spiral interplanetary magnetic field (IMF) orientations corresponding to a wide range of solar wind plasma conditions. To study the growth of the Kelvin-Helmholtz instability on the dawn and dusk flank magnetopause, we have performed 26 local two-dimensional MHD simulations, with the initial conditions taken from global simulations on both sides of the velocity shear layer at the dawn-dusk terminator. These simulations indicate that while the MHD physics of the fast shocks does not directly lead to strong asymmetry of the magnetosheath temperature for typical solar wind conditions, the magnetosheath on the quasi-parallel shock side has a smaller tangential magnetic field along the magnetosheath flow which enables faster growth of the Kelvin-Helmholtz instability (KHI). Because the IMF is statistically mostly in the PS orientation, the KHI formation may statistically favor the dawnside flank. For all the 26 simulations, the growth rates of the KHI correlated well with the ratio of the velocity shear and Alfvén speed along the wave vector, k. Dynamics of the KHI may subsequently lead to formation of kinetic Alfvén waves and reconnection in the Kelvin-Helmholtz vortices which can lead to particle energization. This may partly help to explain the observed plasma sheet asymmetry of cold-component ions, which are heated more on the dawnside plasma sheet.

Citation: Nykyri, K. (2013), Impact of MHD shock physics on magnetosheath asymmetry and Kelvin-Helmholtz instability, *J. Geophys. Res. Space Physics*, *118*, 5068–5081, doi:10.1002/jgra.50499.

1. Introduction

[2] *Hasegawa et al.* [2003] and *Wing et al.* [2005] showed that the cold-dense plasma sheet [*Fairfield et al.*, 1981; *Lennartsson*, 1992] has a strong dawn-dusk asymmetry during northward interplanetary magnetic field (IMF) conditions. The plasma sheet ions have two components: hot (magnetospheric origin) and cold (magnetosheath origin) [*Hasegawa et al.*, 2003, 2004a; *Wing et al.*, 2005]. The temperatures of the cold-component ions in the plasma sheet are 30–40% higher in the dawn sector compared to the dusk sector, implying the dawnside magnetosheath ion heating. As a result, the magnetosheath ions are less distinguishable from the hot-component ions, which have lower temperatures on the dawnside. On the duskside the cold-component ions and hot component ions are more easily distinguishable [*Wing et al.*, 2005; *Hasegawa et al.*, 2003].

[3] The observed dawn-dusk asymmetry of the ion temperatures may be indicative of the entry mechanism generating the cold-dense plasma sheet or indicative of a source (magnetosheath) plasma temperature asymmetry. The cold-dense plasma sheet has been proposed to arise from double high-latitude reconnection [*Song and Russell*, 1992; *Russell et al.*, 2000; *Onsager et al.*, 2001; *Song et al.*, 2003; *Li et al.*, 2005; *Oieroset et al.*, 2005; *Lavraud et al.*, 2005], diffusive processes such as ion mixing due to Kelvin-Helmholtz instability (KHI) [*Fujimoto and Terasawa*, 1994, 1995; *Thomas and Winske*, 1993; *Cowee et al.*, 2010], and reconnection inside KH vortices [*Nykyri and Otto*, 2001, 2004]. *Taylor et al.* [2008] show observational evidence of both high-latitude reconnection and KHI contributing to the formation of the cold-dense plasma sheet.

[4] The statistical studies by *Wing et al.* [2005] and *Hasegawa et al.* [2003] have not taken into account the horizontal component of the IMF. Statistically, the IMF orientation in the equatorial plane is mostly Parker spiral, which would generate the quasi-parallel bow shock on the dawnside and quasi-perpendicular bow shock on the duskside. The quasi-parallel bow shock and the magnetosheath downstream from the shock are very turbulent regions with a variety of wave modes, instabilities, and wave-particle interactions that could heat ions [*Eastwood et al.*, 2002; *Eastwood et al.*, 2003; *Eastwood et al.*, 2004; *Eastwood*

[1]Department of Physical Sciences, Embry-Riddle Aeronautical University, Daytona Beach, Florida, USA.

Corresponding author: K. Nykyri, Department of Physical Sciences, Embry-Riddle Aeronautical University, 600 S. Clyde Morris Blvd., Daytona Beach, FL 32114, USA. (nykyrik@erau.edu)

2169-9380/13/10.1002/jgra.50499

et al., 2005; *Blanco-Cano et al.*, 2006]. Therefore, there might be a statistical asymmetry in the ion temperatures already present in the magnetosheath due to these wave particle-interactions on the quasi-parallel bow shock. Indeed, a recent study by *Walsh et al.* [2012] utilized Time History of Events and Macroscale Interactions during Substorms (THEMIS) data during 2008–2010 just outside the magnetopause in the dayside magnetosheath showing that proton temperature is greater on the dawnside magnetosheath close to magnetopause.

[5] Also, it is well known that the magnetopause is more oscillatory on the morning side [*Russell et al.*, 1997] and this has been attributed to the effect of these enhanced fluctuations originating from the quasi-parallel shock. This may result in (a) more seed fluctuations driving the KHI at the magnetopause or (b) producing reconnection directly if the magnetosheath magnetic field is antiparallel to the magnetospheric field in the shear flow plane [*Chen et al.*, 1997].

[6] In addition, compression and draping of the Parker spiral IMF would generate a stronger tangential magnetic field on the duskside magnetosheath, which is observed recently in a statistical study utilizing THEMIS data during 2007–2012 [*Dimmock and Nykyri*, 2013]. A strong tangential magnetic field along the tail flank could stabilize the Kelvin-Helmholtz (KH) modes with k vectors aligned with this field reducing the plasma transport associated with reconnection in Kelvin-Helmholtz vortices [*Nykyri and Otto*, 2001, 2004].

[7] In the present work, we study the effect of the MHD shock physics and SW plasma conditions on the magnetosheath properties and KHI, but in the real magnetosheath and magnetopause, the temperature asymmetry may be produced by wave heating (which is not present in the MHD) favoring more the turbulent quasi-parallel shock side. The statistical study by *Yao et al.* [2011] supports this statement showing that the spectral energy densities of ion gyroradii-scale electromagnetic waves across the magnetopause are larger on the dawn (412 magnetic local time (MLT)) than duskside (1220 MLT).

[8] The KH mode is driven by a gradient or shear in the plasma velocity which causes wave motion and velocity vortices (in the nonlinear state) on the plasma boundary. However, the presence of a magnetic field component aligned with the **k** vector of the instability stabilizes the mode because it requires additional energy to twist the magnetic field in the boundary or vortex motion. The onset condition for the KH mode is [e.g., *Chandrasekhar*, 1961]

$$\frac{m_0 n_1 n_2}{n_1 + n_2} [\mathbf{k} \cdot \Delta \mathbf{V}]^2 > \frac{1}{\mu_0} \left[(\mathbf{k} \cdot \mathbf{B}_1)^2 + (\mathbf{k} \cdot \mathbf{B}_2)^2 \right], \quad (1)$$

where m_0 is the ion mass, n is the number density, $\Delta \mathbf{V} = (\mathbf{V}_1 - \mathbf{V}_2)$ is the velocity shear, **B** is the magnetic field strength, and the subscripts denote plasma properties on the two sides of the boundary. In a plasma with constant density and constant $|\mathbf{k} \cdot \mathbf{B}|$, this relation becomes

$$(\mathbf{k} \cdot \mathbf{V}_0)^2 > (\mathbf{k} \cdot \mathbf{v}_A)^2 , \quad (2)$$

with $\mathbf{V}_0 = \frac{1}{2} (\mathbf{V}_1 - \mathbf{V}_2)$. Thus, the velocity shear along **k** must be larger than the Alfvén speed along **k** for instability. Note that **B** can reverse along **k**.

[9] Magnetic reconnection requires antiparallel field components across a current sheet. However, reconnection is entirely switched off if the shear velocity is larger than the local Alfvén speed because the information that reconnection operates propagates with Alfvén speed along the magnetic field [*Chen et al.*, 1997]. Therefore, if the plasma flow is faster than the local Alfvén speed, this information cannot propagate away from the reconnection side [*Chen et al.*, 1997]. Properties of reconnection and KH modes alter in asymmetric plasma conditions but the qualitative physics remains the same. There have been numerous numerical simulation studies of the Kelvin-Helmholtz instability in the past. These simulations are carried out using MHD [*Miura and Pritchett*, 1982; *Miura*, 1984, 1987, 1992; *Chen et al.*, 1997; *Keller and Lysak*, 1999; *Otto and Fairfield*, 2000; *Nykyri and Otto*, 2001], Hall-MHD [*Huba*, 1994, 1996; *Fujimoto and Terasawa*, 1991; *Nykyri and Otto*, 2004], hybrid, and kinetic codes [*Terasawa et al.*, 1992; *Thomas and Winske*, 1993; *Fujimoto and Terasawa*, 1994, 1995; *Thomas*, 1995]. The main objective of these studies has been to understand the nonlinear evolution of the KH instability at the magnetopause and its effect on the momentum, energy and plasma transport, and diffusion at the thin boundaries generated by the KHI.

[10] Before these nonlinear numerical simulations were possible, there were many hydrodynamic and magnetohydrodynamic linear stability studies in compressional plasma assuming an infinitely thin boundary layer [see, e.g., *Pu and Kivelson*, 1983, and references therein]. According to many of these studies, there is an upper velocity limit or sonic Mach number above which the KHI is stabilized, which would suggest that a great portion of the tail flanks would be stable to the KHI. However, *Miura* [1990] demonstrated that when the boundary layer thickness is finite and the criteria in equation (2) is satisfied, the flank boundary is always KH unstable regardless of the sonic Mach number. However, the thicker the boundary, the longer the wavelength of the fastest-growing mode. *Miura* [1992] further showed that the boundary layer becomes wider and more nonlinearly corrugated by the instability for smaller sonic Mach numbers.

[11] Also, most (except *Thomas* [1995]) of the older works [*Fujimoto and Terasawa*, 1991; *Terasawa et al.*, 1992; *Thomas and Winske*, 1993; *Fujimoto and Terasawa*, 1994, 1995; *Huba*, 1994, 1996] that include the ion inertia term or finite Larmor radius effect in their simulations use a perpendicular ($\mathbf{V_0} \perp \mathbf{B}$) configuration or a linearized set of extended MHD equations, or both. A case where magnetic field is exactly perpendicular to shear flow plane is singular, and therefore, simulations describing more realistically KHI at the magnetospheric boundary must include magnetic field components both perpendicular and parallel to the k vector.

[12] There have been also various spacecraft observations of the Kelvin-Helmholtz instability at the low-latitude boundary layer (LLBL) [e.g., *Fairfield et al.*, 2000; *Nykyri et al.*, 2003; *Hasegawa et al.*, 2004b; *Fairfield et al.*, 2007; *Taylor et al.*, 2008; *Hwang et al.*, 2011] as well as observations of reconnection produced by KHI [*Nykyri et al.*, 2006; *Hasegawa et al.*, 2009]. This transport mainly occurs due to the twisting of the magnetic field B inside the Kelvin-Helmholtz vortex which leads to the magnetic reconnection and detachment of the plasma blobs that can produce

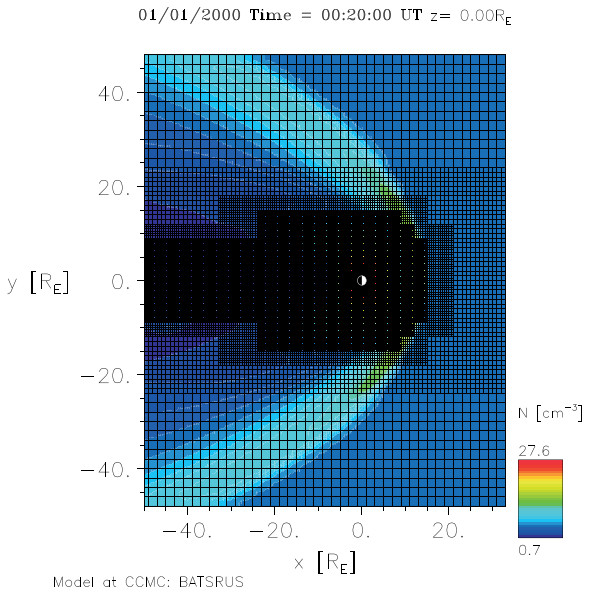

Figure 1. The grid in x, y plane used for all global simulation runs for cases 1–10. Background color depicts plasma density for case 1a.

diffusion coefficients on the order of 10^9 m^2/s, which is sufficient for generating the cold-dense plasma sheet during strongly northward IMF orientations [*Otto and Fairfield*, 2000; *Nykyri and Otto*, 2001, 2004].

[13] There is also another possible magnetic field configuration resulting in reconnection due to the KHI. *Nakamura et al.* [2006] and *Nykyri et al.* [2006] showed that when the tangential magnetic fields are initially antiparallel over the velocity shear layer, the reconnection can operate in two regions within the vortex: (a) in the current layer separating magnetosheath and magnetospheric fields and (b) in the current layer generated by the twisting of the KHI.

[14] The Cluster observations of the KHI on the dawn flank reported by *Nykyri et al.* [2006] occurred during Parker spiral (PS) IMF orientation. The best model-data comparison was achieved when the simulation k vector was tilted by 35°, thus increasing the ratio of shear flow and Alfvén speed tangential to the k vector with respect to a 0° tilt case and creating a finite k_z. Utilizing 5 years of Cluster data (2001–2005) during several hundred magnetopause boundary crossings at the LLBL, we have since found five new events (not previously published in literature) of the KHI occurring on the dawn flank magnetopause. All these new events occurred predominantly during a PS IMF orientation [*Moore*, 2012]. Considering the sample size of only $\approx$ 10 published KH events observed with in situ spacecraft observations at the Earth's LLBL, these five new cases together with the *Nykyri et al.* [2006] event form about 40% of all the events.

[15] The present paper is therefore strongly motivated by these recent observations of the KHI on the dawn flank magnetopause during PS IMF and the observed dawn-dusk plasma sheet temperature asymmetries. In this work, we will focus on addressing the impact of the magnetosheath properties arising from MHD shock physics on the growth of the Kelvin-Helmholtz instability at the magnetopause boundary. We present the results of a series of global MHD simulations of magnetosheath properties for Parker spiral (PS) and ortho-Parker spiral (OPS) IMF orientations for different solar wind plasma parameters and initialize local 2-D MHD simulations at the magnetopause flanks corresponding to these magnetosheath conditions to study the growth of the KHI.

[16] We chose this approach because modeling the KHI directly in the global MHD simulations is very difficult due to large system size and the fine numerical resolution required to resolve the magnetopause. In order to study the details of the KHI, the numerical diffusion of the code (which depends on the grid resolution) should be less than the diffusion produced by the KHI (less than 10^9 m^2/s). For example, *Fairfield et al.* [2007] compared Geotail observations of the KHI during an extended period of northward IMF orientation with the Block Adaptive Tree Solar Wind–Roe–Upwind Scheme (BATS-R-US) global model utilizing computationally expensive specialized 1/16 R_E resolution (not currently available in Community Coordinated Modeling Center (CCMC) "runs on request" website). Despite this relatively high resolution, their simulation only produced linear waves that did not reach nonlinear stage as observed in the Geotail data.

[17] Also other authors have studied KHI in global codes both during southward [*Claudepierre et al.*, 2008; *Hwang et al.*, 2011] and northward [*Guo et al.*, 2010; *Li et al.*, 2012] IMF orientations. These studies were able to study the large-scale structure of the magnetopause oscillations and spectral power of oscillations [*Claudepierre et al.*, 2008], and some were able to determine the phase speeds and wavelengths

Table 1. Global MHD Simulation Runs

	B (nT)	**V** (km/s)	n (1/cm^3)	T (10^5 K)	β	$P_{\rm dyn}$ (nPa)	M_A	M_{MS}
Case 1a (PS)	5,–5,5	–400,0,0	5	2	0.46	1.34	4.73	4.02
Case 1b (PS2)	–5,5,5	–400,0,0	5	2	0.46	1.34	4.73	4.02
Case 1c (OPS)	5,5,5	–400,0,0	5	2	0.46	1.34	4.73	4.02
Case 1d (OPS2)	–5,–5,5	–400,0,0	5	2	0.46	1.34	4.73	4.02
Case 2 (PS)	5,–5,5	–600,0,0	5	2	0.46	3.00	7.10	6.03
Case 3 (PS)	5,–5,5	–600,0,0	3	2	0.28	1.80	5.50	4.95
Case 4 (PS)	3.5,–3.5,0	–600,0,0	20	2	5.67	12.02	24.83	10.38
Case 5 (PS)	3.5,–3.5,0	–400,0,0	5	2	1.42	1.34	8.28	5.61
Case 6 (PS)	2.5,–2.5,0	–350,0,0	2.5	0.3	0.21	0.51	7.17	6.62
Case 7 (PS)	10,–10,10	–400,0,0	3	2	0.069	0.80	1.83	1.78
Case 8 (PS)	10,–10,10	–400,0,0	5	2	0.12	1.34	2.37	2.26
Case 9 (PS)	10,–10,10	–400,0,0	10	2	0.23	2.67	3.35	3.06
Case 10 (PS)	10,–10,10	–400,0,0	20	2	0.46	5.34	4.73	4.02

Table 2. Plasma Parameters Across the Velocity Shear Layer

	y (R_E)	$\mathbf{B_k}$ (nT)	$\mathbf{B}_\perp$ (nT)	φ (deg)	$\mathbf{V_k}$ (km/s)	n (1/cm^3)	T (10^5 K)	β	$v_{\rm shear}/\mathbf{v_A}\cdot\mathbf{k}$	$v_{\rm shear}/\mathbf{v_{MS}}\cdot\mathbf{k}$	$v_{\rm shear}/v_{A_{\rm ave}}$
	Dawn/Dusk	Dawn/Dusk	Dawn/Dusk	Dawn/Dusk	Dawn/Dusk	Dawn/Dusk	Dawn/Dusk	Dawn/Dusk	Dawn/Dusk	Dawn/Dusk	Dawn/Dusk
Case 1a (PS) MSH	–16.0/ 16.0	6.6/ –14.7	21.2/ 18.9	17.3/ –37.9	284.3/ 301.0	6.4/ 6.3	18.9/ 17.8	0.8/ 0.7	4.95/ –2.30	2.22/ 1.74	1.48/ 1.41
MSP	–12.8/ 12.8	2.5/ –2.4	21.1/ 22.4	6.7/ –6.2	2.3/ 6.7	6.0/ 5.6	33.7/ 35.4	1.5/ 1.3	12.67/ –13.19	1.84/ 1.87	
Case 1b (PS2) MSH	–16.0/ 16.0	–6.6/ 14.7	21.2/ 18.9	–17.3/ 37.9	284.3/ 301.0	6.4/ 6.3	18.9/ 17.8	0.8/ 0.7	–4.95/ 2.30	2.22/ 1.74	1.48/ 1.41
MSP	–12.8/ 12.8	–2.5/ 2.4	21.1/ 22.4	–6.7/ 6.2	2.3/ 6.7	6.0/ 5.6	33.7/ 35.4	1.5/ 1.3	–12.67/ 13.19	1.84/ 1.87	
Case 1c (OPS) MSH	–16.0/ 16.0	–14.7/ 6.6	18.9/ 21.2	–37.9/ 17.3	301.0/ 284.3	6.3/ 6.4	17.8/ 18.9	0.7/ 0.8	–2.30/ 4.95	1.74/ 2.22	1.41/ 1.48
MSP	–12.8/ 12.8	–2.4/ 2.5	22.4/ 21.1	–6.2/ 6.7	6.7/ 2.3	5.6/ 6.0	35.4/ 33.7	1.3/ 1.5	–13.19/ 12.67	1.87/ 1.84	
Case 1d (OPS2) MSH	–16.0/ 16.0	14.7/ –6.6	18.9/ 21.2	37.9/ –17.3	301.0/ 284.3	6.3/ 6.4	17.8/ 18.9	0.7/ 0.8	2.30/ –4.95	1.74/ 2.22	1.41/ 1.48
MSP	–12.8/ 12.8	2.4/ –2.5	22.4/ 21.1	6.2/ –6.7	6.7/ 2.3	5.6/ 6.0	35.4/ 33.7	1.3/ 1.5	13.19/ –12.67	1.87/ 1.84	
Case 2 (PS) MSH	–14.4/ 14.4	9.0/ –18.0	26.1/ 23.5	19.0/ –37.5	416.3/ 432.3	7.4/ 7.3	41.9/ 40.3	1.4/ 1.2	5.78/ –2.98	2.26/ 1.96	1.73/ 1.69
MSP	–11.2/ 11.2	3.7/ –3.9	29.2/ 30.0	7.1/ –7.5	3.9/ 3.8	6.1/ 5.8	72.9/ 76.6	1.8/ 1.7	12.93/ –12.11	1.84/ 1.86	
Case 3 (PS) MSH	–16.0/ 16.0	7.6/ –16.5	22.0/ 19.2	18.9/ –40.6	418.8/ 436.4	4.6/ 4.5	39.3/ 37.5	1.2/ 0.9	5.04/ –2.29	2.14/ 1.66	1.54/ 1.41
MSP	–12.8/ 12.8	3.1/ –3.2	23.2/ 24.4	7.5/ –7.4	31.0/ 47.0	3.7/ 3.4	68.0/ 71.4	1.6/ 1.4	11.12/ –10.40	1.77/ 1.73	
Case 4 (PS) MSH	–11.2/ 11.2	7.2/ –14.1	18.5/ 17.7	21.2/ –38.6	414.8/ 418.9	33.9/ 33.7	48.8/ 48.4	16.6/ 11.5	17.48/ –8.93	2.54/ 2.49	1.92/ 1.89
MSP	–8.0/ 8.0	3.9/ –5.4	66.0/ 66.2	3.4/ –4.7	–57.0/ –57.2	12.2/ 12.1	114.0/ 115.0	1.1/ 1.1	19.11/ –13.94	1.67/ 1.67	
Case 5 (PS) MSH	–16.0/ 16.0	7.1/ –12.5	7.6/ 5.8	42.8/ –65.1	254.6/ 271.3	7.7/ 7.5	23.2/ 22.0	6.0/ 3.0	4.89/ –2.88	1.97/ 1.81	2.17/ 2.01
MSP	–12.8/ 12.8	3.3/ –3.8	15.8/ 16.5	11.6/ –12.8	–19.5/ –17.2	4.3/ 4.4	41.0/ 41.4	2.4/ 2.2	7.98/ –7.33	1.59/ 1.66	
Case 6 (PS) MSH	–19.2/ 19.2	5.0/ –9.0	3.4/ 2.4	56.2/ –74.8	215.9/ 235.2	4.3/ 4.1	16.1/ 15.0	6.8/ 2.4	4.64/ –2.69	2.08/ 1.87	2.71/ 2.25
MSP	–14.4/ 14.4	1.7/ –2.2	9.4/ 10.2	10.5/ –12.5	–30.9/ –29.1	3.1/ 3.0	23.3/ 25.0	2.8/ 2.4	11.47/ –9.17	1.90/ 1.95	
Case 7 (PS) MSH	–16.0/ 16.0	6.3/ –20.1	25.1/ 21.6	14.2/ –42.9	321.8/ 343.3	3.8/ 3.4	15.6/ 10.0	0.3/ 0.1	4.53/ –1.28	2.55/ 1.21	1.22/ 0.94
MSP	–12.8/ 12.8	4.6/ –3.6	24.2/ 27.2	10.7/ –7.6	3.1/ 38.1	5.2/ 4.0	30.0/ 35.6	0.9/ 0.7	7.31/ –7.70	2.12/ 1.89	
Case 8 (PS) MSH	–14.4/ 14.4	8.2/ –20.5	27.4/ 25.8	16.7/ –38.6	300.4/ 342.8	5.6/ 5.1	21.4/ 16.5	0.5/ 0.3	3.24/ –1.75	1.72/ 1.54	0.97/ 1.16
MSP	–12.8/ 11.2	4.6/ –4.4	26.4/ 34.1	9.8/ –7.4	53.9/ –5.7	5.8/ 7.3	34.7/ 32.0	1.0/ 0.7	5.95/ –9.74	1.54/ 2.28	
Case 9 (PS) MSH	–14.4/ 14.4	9.5/ –26.0	34.8/ 29.4	15.2/ –41.5	304.4/ 311.3	13.3/ 12.9	15.0/ 14.0	0.5/ 0.4	5.15/ –1.79	2.52/ 1.52	1.28/ 1.12
MSP	–11.2/ 11.2	4.6/ –4.8	34.7/ 36.7	7.6/ –7.5	11.8/ 28.7	10.1/ 9.3	38.0/ 41.4	1.1/ 1.0	9.16/ –8.15	1.78/ 1.64	
Case 10 (PS) MSH	–12.8/ 12.8	12.9/ –29.7	41.4/ 36.4	17.3/ –39.3	290.6/ 304.2	26.9/ 26.6	17.6/ 16.6	0.9/ 0.7	5.42/ –2.44	2.40/ 1.86	1.42/ 1.37
MSP	–9.6/ 9.6	6.0/ –6.8	47.1/ 48.8	7.2/ –7.9	–4.9/ –3.4	19.9/ 18.7	38.6/ 41.2	1.2/ 1.1	10.09/ –8.95	1.78/ 1.78	

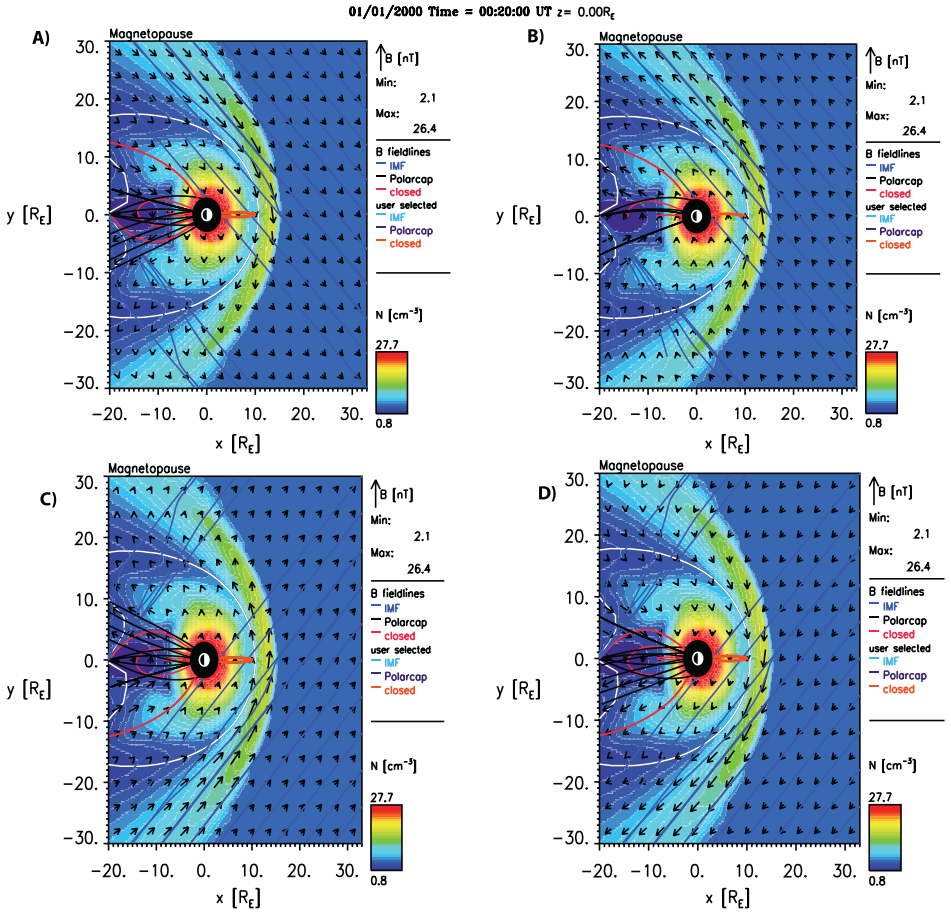

Figure 2. The plasma number density, magnetic field vectors, and magnetic field lines for cases 1a–1d, respectively. The shape of the Earth (also in Figures 3–6) is slightly elongated due to larger plot view in *y* dimension.

albeit using only a quarter system and ignoring the effects of the magnetosphere-ionosphere (M-I) coupling [*Li et al.*, 2012].

[18] Currently, there are no previous works studying KHI in global codes during a PS and OPS IMF orientation. Studying the KHI during a PS and OPS IMF orientation in global MHD codes that include M-I coupling and that can simultaneously resolve the KHI at the flanks and high-latitude reconnection would be crucial in order to fully address the dawn-dusk asymmetries arising from asymmetric evolution of these processes and their mutual interaction. However, this study would require higher numerical resolution than currently available in CCMC "runs on request" website.

[19] The present paper is organized as follows: section 2 presents the numerical models used in this study; section 3 lists the input parameters of all the runs in the global MHD model and shows the results of the magnetosheath plasma and field properties for these runs; section 4 shows the results and growth times of the local 2-D MHD simulations of the KHI; and section 5 discusses and concludes the findings of the study.

2. Numerical Method

2.1. Global 3-D MHD Simulations

[20] This study utilizes the Block Adaptive Tree Solar Wind–Roe–Upwind Scheme (BATS-R-US) global MHD simulation originally developed by the MHD group at the University of Michigan [*Tóth et al.*, 2005]. The BATS-R-US code solves 3-D MHD equations in finite volume form using numerical methods related to Roe's Approximate Riemann Solver. The code uses an adaptive grid composed of rectangular blocks arranged in varying degrees of spatial refinement levels. All the BATS-R-US runs (Space Weather Modeling Framework version v8.01) used in this study are available for viewing at NASA Community Coordinated Modeling Center (CCMC). In order to solely focus on the asymmetries generated by the quasi-parallel versus quasi-perpendicular MHD shock physics on the magnetosheath, we have assumed 0° dipole tilt, have not included Rice Convection Model (RCM), have assumed constant ionospheric conductances and zero radio flux, and have kept solar wind input constant throughout each 1 h run. We use the standard grid with 1,958,688 number of cells. Figure 1 shows the system size and the adaptive grid in the x, y (GSM) plane. The finest grid resolution is 1/4 R_E surrounded by 1/2 R_E resolution grid, which is enveloped by a 1 R_E resolution grid. This in turn is enveloped by a 2 R_E resolution grid extending up to $x = -135$ R_E where the resolution is further reduced. Table 1 presents the input parameters for 13 global MHD simulations with SW plasma betas (β) varying from 0.069 to 5.67 and Alfvén and magnetosonic Mach numbers varying from 1.83 to 24.83 and 1.78 to 10.38, respectively. In order for

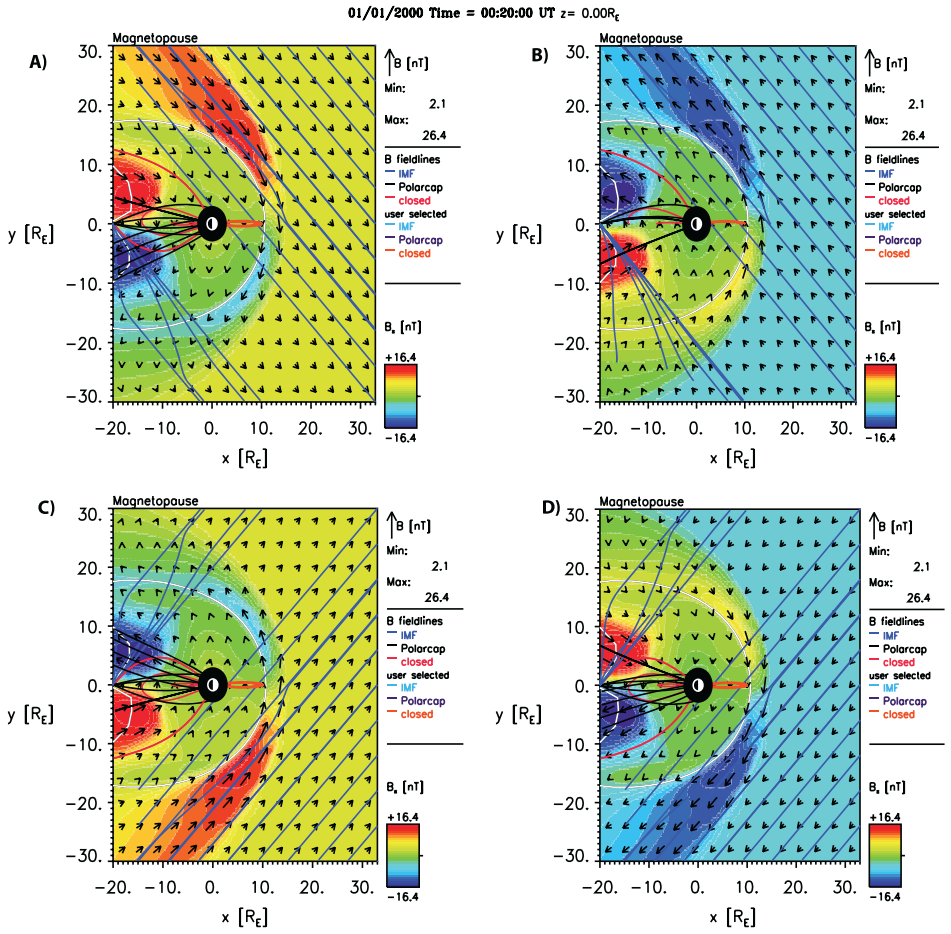

Figure 3. The x component of the magnetic field, magnetic field vectors, and magnetic field lines for cases 1a–1d, respectively.

the magnetosheath-magnetosphere system to reach a steady state, we use the 1 h duration global simulation results at time = 20 min after initializing the run.

2.2. Local 2-D MHD Simulations

[21] The evolution of the Kelvin-Helmholtz instability in this study is obtained with 2.5-dimensional high-resolution MHD simulations [*Otto*, 1990; *Otto and Fairfield*, 2000; *Nykyri and Otto*, 2001; *Nykyri et al.*, 2006] in the x,y plane (approximately the equatorial plane for strongly northward IMF). The initial configuration for the simulation in the boundary coordinates uses a magnetic field of $b_{x0}(x) = b_0(x)\sin\varphi$, $b_{y0}(x) = 0$, and $b_{z0}(x) = b_0(x)\cos\varphi$ such that $90° - \varphi$ is the angle between the unperturbed magnetic field direction and the **k** vector of the KH mode. Initial density, pressure, velocity, and magnetic field direction on the magnetospheric and magnetosheath side are chosen at the dawn-dusk terminator at both sides of the velocity shear layer from global MHD simulations. The simulation length scale, L_0 = 1000 km, is normalized to typical magnetopause thickness at the dayside magnetopause. The velocity shear layer thickness, Δ, is set to $3L_0$ = of 3000 km, although in global simulations this thickness is typically 3–4 R_E, which is due to lower numerical resolution than the local code. The system size in the local simulations is $[y,x] = 80 \times 40L_0$, with a larger system size perpendicular (y axis in Figures 8 and 9) to the initial current layer. The vertical scale is chosen to study the evolution of the fastest-growing mode with a wavelength of $\lambda \approx 4\pi\Delta$ [*Miura and Pritchett*, 1982]. The simulations use an adjustable grid with 403 × 203 grid points with maximum resolution of a 0.05 in the center of the simulation box corresponding to a 50 km spatial resolution with our choice of L_0. The simulations use fixed (periodic) boundary conditions perpendicular (along) to the initial current layer separating the magnetosheath and magnetospheric plasma.

[22] Table 2 presents the values at the dawn-dusk terminator on the both sides (magnetosheath (MSH) and magnetosphere (MSP)) of the velocity shear layer that are used to generate the local MHD simulations. The columns from left to right show (1) the y location for data collection in both sides of the velocity shear layer; (2) the magnetic field along the k vector of the KHI taken as the horizontal magnetic field component in x,y plane ($B_k = \sqrt{b_x{}^2 + b_y{}^2}$) and taken as positive if along the magnetosheath flow and negative when antiparallel to the magnetosheath flow; (3) the vertical magnetic field component with respect to the x,y plane ($B_\perp$); (4) the angle (φ) between the magnetic field and the direction vertical to the x,y plane ($\varphi = \mathrm{atan}(B_k/B_\perp)$) taken as positive when the field tilts tailward and negative if sunward; (5) the horizontal velocity component in the x,y plane ($V_k = \sqrt{v_x{}^2 + v_y{}^2}$) which is taken as positive when tailward and negative when sunward (the velocity

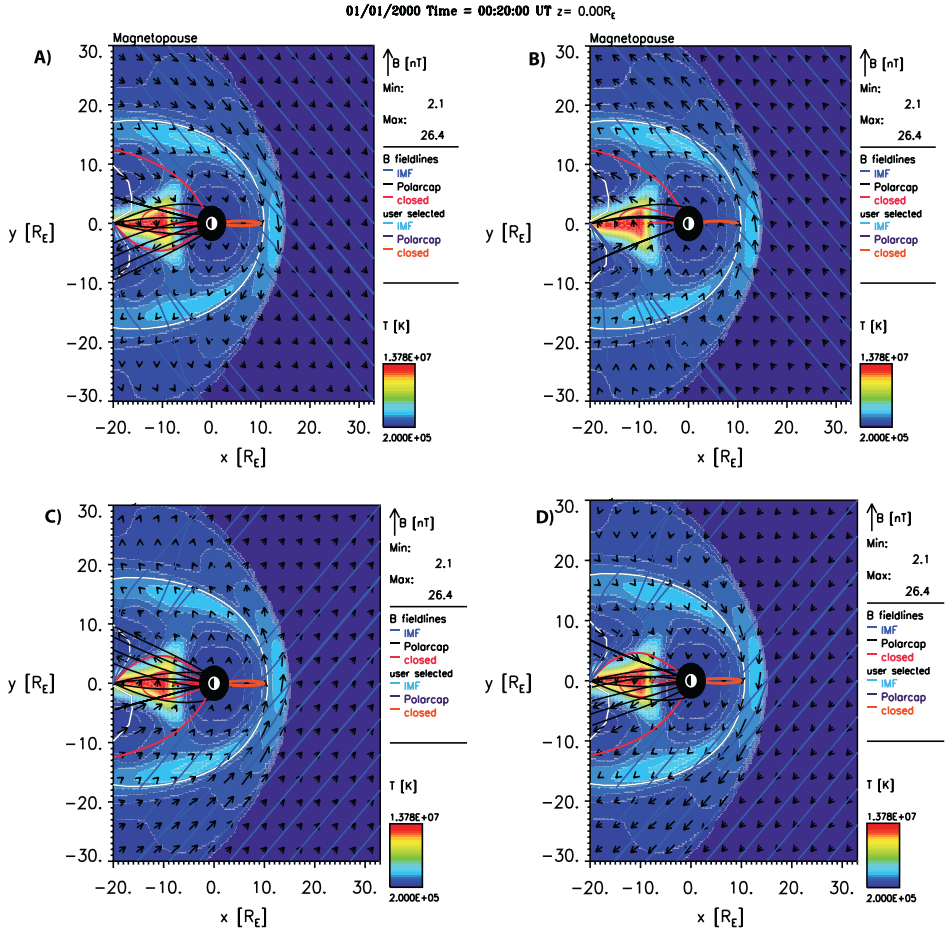

Figure 4. The plasma temperature, magnetic field vectors, and magnetic field lines for cases 1a–1d, respectively.

shear is then determined from $v_{\text{shear}} = V_{k_{\text{MSH}}} - V_{k_{\text{MSP}}}$); (6) plasma number density (n); (7) plasma temperature (T); (8) plasma beta (β); (9) ratio between the velocity shear and horizontal Alfvén speed ($v_{\text{shear}}/(B_k/\sqrt{\mu_0 n m_p})$; (10) ratio between the velocity shear and "horizontal" magnetosonic speed ($v_{\text{shear}}/(\sqrt{V_s^2 + B_k^2/(\mu_0 n m_p)})$), where V_s stands for sound speed; and (11) $V_{A_{\text{ave}}}$ the average Alfvén speed across the velocity shear layer.

3. Magnetosheath Properties for PS and OPS IMF Orientations

[23] Global MHD runs 1a–1d (see Table 1) all have the same magnetic field strength and typical solar wind plasma conditions but differ in magnetic field orientation in the x,y plane. All of these runs are for the northward IMF orientation but runs 1a and 1b are created for two Parker spiral (PS and PS2) orientations and 1c and 1d are for two ortho-Parker spiral (OPS and OPS2) orientations, respectively. Because we have not included the dipole tilt, the PS and OPS runs have a mirror symmetry with respect to x axis such that the dawnside magnetosheath (MSH) flank for PS and PS2 orientation has the same plasma and field properties as the duskside magnetosheath for OPS and OPS2 orientations, respectively (see plasma and field quantities collected at dawn-dusk terminator on the magnetospheric and magnetosheath side of the velocity shear layer in Table 2).

[24] Figures 2–6 show the global MHD results for runs 1a–1d in the x,y plane with a background color depicting the plasma number density (Figure 2), x component of the magnetic field (Figure 3), plasma temperature (Figure 4), plasma beta (Figure 5), and Alfvén Mach number (Figure 6). The arrows show the magnetic field vectors and the lines are the magnetic field lines. For a PS (OPS) orientation, the quasi-parallel bow shock is on the dawnside (duskside) and quasi-perpendicular shock is on the duskside (dawnside) making the magnetic field more (less) compressed on the duskside (dawnside).

[25] As expected from the Rankine-Hugoniot equations, on the exactly parallel shock, there is a compression of the plasma but not the magnetic field, while on the perpendicular shock, both are compressed. Figure 2 indicates that the plasma number density is only slightly enhanced (larger light green area at dawn MSH at $x < 5\,R_E$) in the magnetosheath corresponding to the quasi-parallel shock side compared to the quasi-perpendicular shock side. Also, the values of number density collected at the dawn-dusk terminator across the velocity shear layer (column 6 in Table 2) are slightly higher on the quasi-parallel shock side.

[26] Figure 3 shows that the x component of the magnetic field is clearly enhanced on the quasi-perpendicular

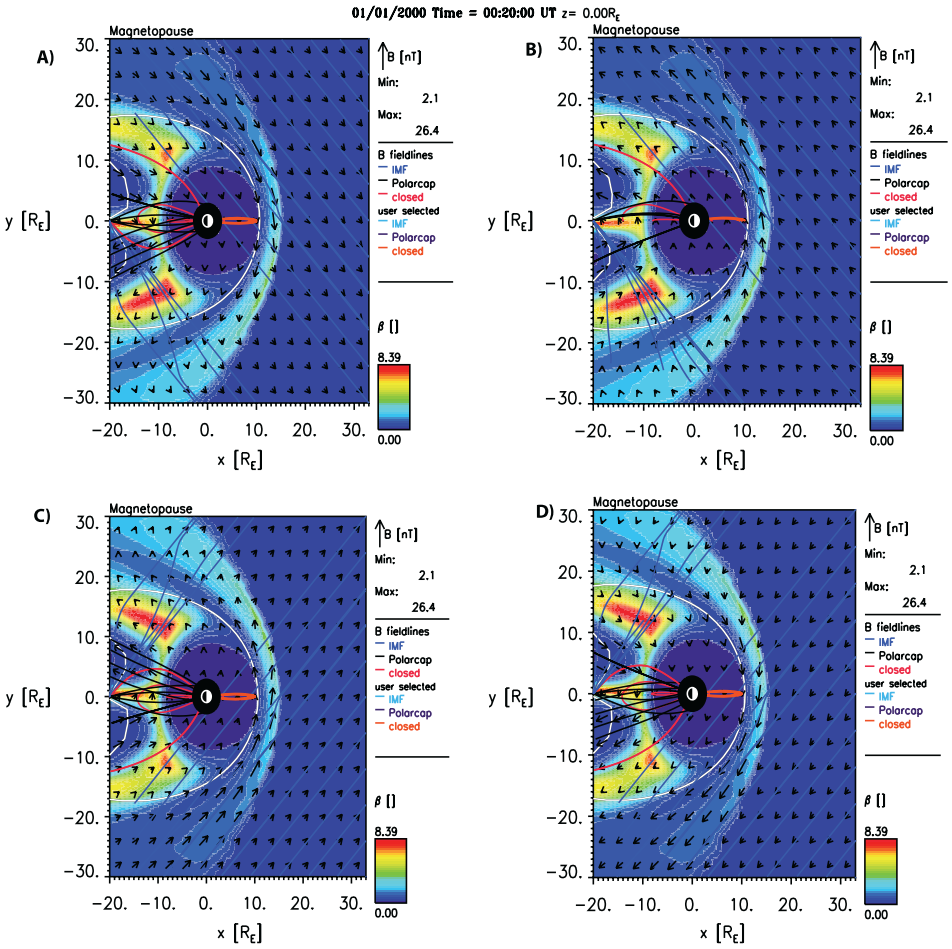

Figure 5. The plasma beta, magnetic field vectors, and magnetic field lines for cases 1a–1d, respectively.

shock side and can act as a stabilizer for instabilities feeding from velocity shear like the Kelvin-Helmholtz instability. The MSH dawn-dusk asymmetry in B_x is produced because of the following reasons. First, during the PS IMF orientation, the IMF is quasi-parallel (perpendicular) to the shock normal on the dawnside (duskside), making the initial upstream IMF more tangential with respect to the magnetopause boundary on the quasi-perpendicular shock side. Second, this tangential field gets further enhanced as the fast shock compresses the magnetic field on the quasi-perpendicular shock, whereas at an exactly parallel shock, there is no compression, and at a quasi-parallel shock, there is a smaller compression of the magnetic field compared to quasi-perpendicular shock side. These effects generate both a stronger magnetic field strength and a larger tangential component of the magnetic field on the duskside (quasi-perpendicular shock side) MSH. Finally, as the MSH field gets draped around the magnetopause, a larger tangential component of the magnetic field forms on the duskside magnetopause compared to the dawn. Note that whether the IMF is in the PS or PS2 orientation (or OPS and OPS2) determines the direction of the magnetic field tangential to the magnetopause boundary which will have an impact on the details of the reconnection driven by Kelvin-Helmholtz instability (see next section).

[27] Figure 4 shows plasma temperature for cases 1a–1d. The MHD shock physics does not seem to result in a strong temperature asymmetry (this does not become visible even after adjusting the color bar). Table 2 (column 7) shows that for the typical SW conditions, the plasma temperatures are only slightly higher in the magnetosheath on the side of the quasi-parallel shock compared to the magnetosheath on the quasi-perpendicular shock side (these values are collected at the dawn-dusk terminator on the MSH side of the velocity shear layer). Only for very low beta solar wind (case 7), the dawnside magnetosheath is about 56% hotter at this one point compared to the dusk. However, this large difference is partly due to the different structure of the velocity shear layer in the dawn compared to the dusk which in general is more complicated for this low beta magnetosheath than for other runs. Figure 7 shows two cuts along the dawn-dusk terminator at $x, z = 0$ for case 1a (Figure 7a) and for case 7 (Figure 7b). For case 1a, the location of the velocity and temperature gradient start approximately at the same point, whereas for case 7, the temperature gradients at the dawn and dusk start at different locations with respect to the steepest gradient in v_x. On the dawn, the location of the steepest gradient in v_x coincides quite well with the steepest temperature gradient at $y = -16\,R_E$, whereas on the dusk terminator, the location of the steepest gradient in v_x is already inside the magnetopause (as indicated by increased plasma temperature) and starts at $y = 14.4\,R_E$. Both on the dawn and dusk, there are two additional temperature gradients at $y = -17.6$ and $y = 17.6$. At the dawn, this point is in

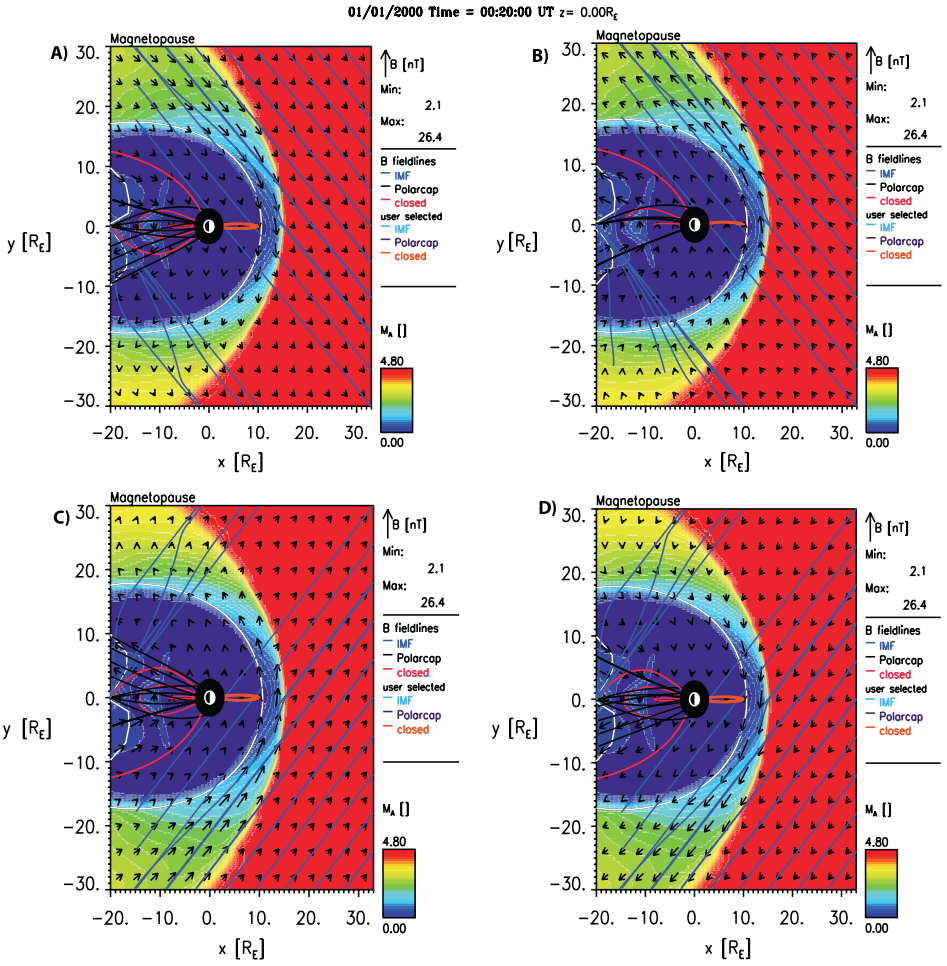

Figure 6. The Alfvén Mach number (M_A), magnetic field vectors and magnetic field lines for cases 1a–1d, respectively.

the region of higher magnetosheath flow than the point at $y = -16$, whereas at the dusk, this point is in the region of the slower magnetosheath flow compared to the accelerated flow next to the magnetopause (where temperature gradient is the largest). If one collects the dawn and dusk temperatures at $|y| = 17.6$, the dawnside magnetosheath temperature is only 23% higher than the temperature at the dusk.

[28] Figure 5 shows that plasma beta in the central magnetosheath is higher on the side of the quasi-parallel shock compared to the quasi-perpendicular shock side due to a larger compression at perpendicular shock which produces

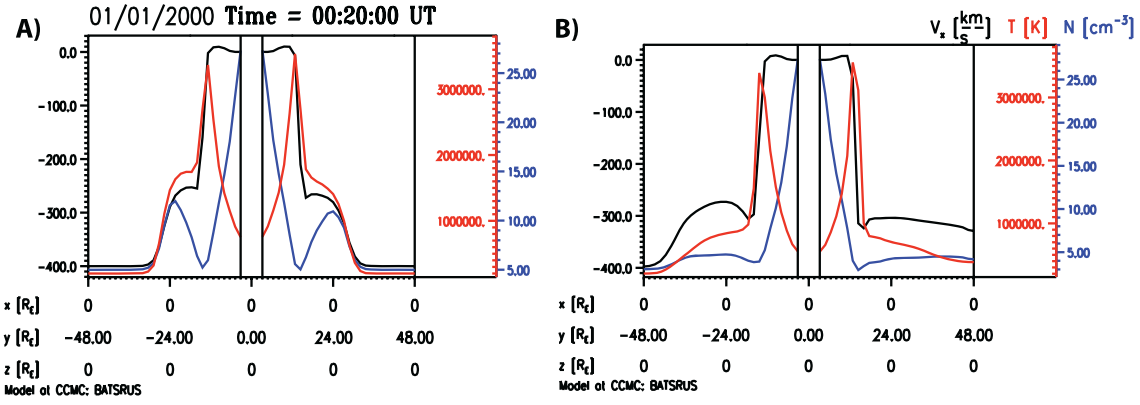

Figure 7. The x component of the plasma velocity, plasma temperature, and number density along y axis for $x, z = 0$ for cases (a) 1a and (b) 7.

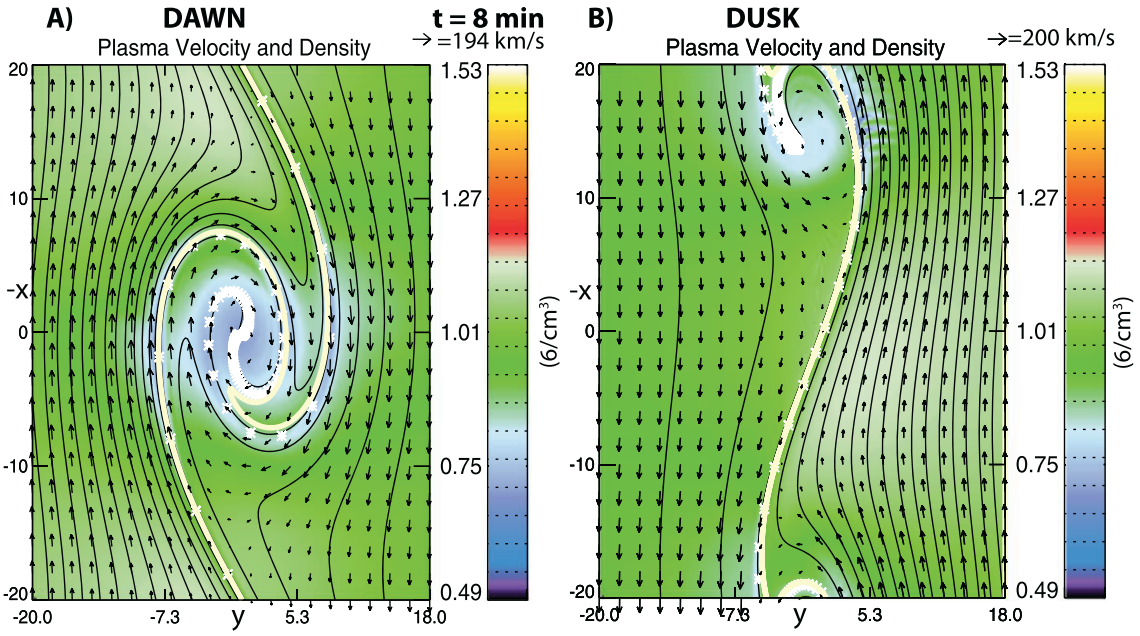

Figure 8. Plasma velocity vectors, density, and magnetic field lines at dawnside flank at t = 8 minutes for case 1a on the (a) dawn and (b) dusk flank respectively. The larger growth rate of the KHI on the dawn flank is evident in the larger scale size of the vortex in Figure 8a (approximately $15L_0$ in y direction and $18L_0$ in x direction) compared to Figure 8b (approximately $6L_0$ in y direction and $7L_0$ in x direction). These simulations correspond to solid and dashed black curves in Figure 10, also confirming that the KHI growth on the dusk flank is slower. All length units are normalized to L_0 = 1000 km.

larger magnetic pressure on quasi-perpendicular MSH. However, there is a layer of lower beta plasma adjacent to the magnetopause also at the side of the parallel and quasi-parallel shock. Table 2 (column 8) shows that plasma beta at the dawn-dusk terminator on the magnetosheath side of the velocity shear layer is higher at the quasi-parallel shock side for all runs.

[29] Figure 6 presents Alfvén Mach number which is lower on the quasi-perpendicular shock side, which is expected due to a stronger magnetic field compression, and higher Alfvén speed, although the plasma flow velocity is slightly larger in the dusk magnetosheath compared to the dawn as can be seen from the tangential velocity (see column 5 in Table 2).

[30] For typical upstream plasma and field values, the MHD shock physics thus does not seem to directly lead to a strong dawn-dusk temperature asymmetry that could explain the magnitude of the observed asymmetry in the temperatures of the cold-component ions more on the dawnside plasma sheet observed in statistical study by *Wing et al.* [2005]. However, the asymmetry in the tangential magnetic field may lead to differences in growth of the physical mechanisms at the magnetopause boundary. In the next section we focus on studying the evolution of the Kelvin-Helmholtz instability (KHI) at the dawn and dusk flank magnetopause for 10 different upstream solar wind conditions.

4. Evolution of the Kelvin-Helmholtz Instability as a Function of Magnetosheath Properties

[31] Figure 7 presents the x component of the plasma velocity, plasma temperature, and number density along the dawn-dusk terminator for cases 1a (Figure 7a) and 7 (Figure 7b). These types of plots are created for each run listed in Table 1 and are used to determine the magnetosheath and magnetospheric locations across the velocity shear layer (sharp gradient in v_x) where the plasma and field values are collected for local simulations. These values used for the local simulation input are recorded in Table 2 both at the dawn and dusk flanks. Because our local MHD simulations need to start from the total pressure equilibrium where the sum of magnetic and plasma pressures in the magnetosheath equals to the total pressure in the magnetosphere $\left(B_1^2/2\mu_0 + n_1kT_1 = B_2^2/2\mu_0 + n_2kT_2\right)$, we have computed the magnetic field pressures at both sides of the velocity shear layer, taken plasma pressure in the magnetosheath, and computed the plasma pressure inside the magnetosphere from the pressure balance. Therefore, the magnetospheric values of plasma beta from the global simulations listed in Table 2 can be slightly different from those computed from the pressure balance.

[32] Figure 8 shows the evolution of the plasma velocity (arrows) and number density (background color) for case 1a on the dawn (Figure 8a) and dusk (Figure 8b) flank, respectively. At time t = 8 min, the boundary is distorted by the Kelvin-Helmholtz instability on the dawn flank whereas the dusk flank is more stable (KH growth is slower) due to a stronger tangential magnetic field. The dusk flank tangential magnetic field is 123% larger compared to the dawn flank magnetosheath as indicated in the first row and second column of Table 2. Although the magnetosheath flow along the dusk flank is slightly larger (by $\sim$ 6%), the stronger tangential magnetic field makes the Alfvén speed along the flow larger making the $v_{\text{shear}}/v_A \cdot k$ ratio 54% smaller at the dusk compared to the dawn.

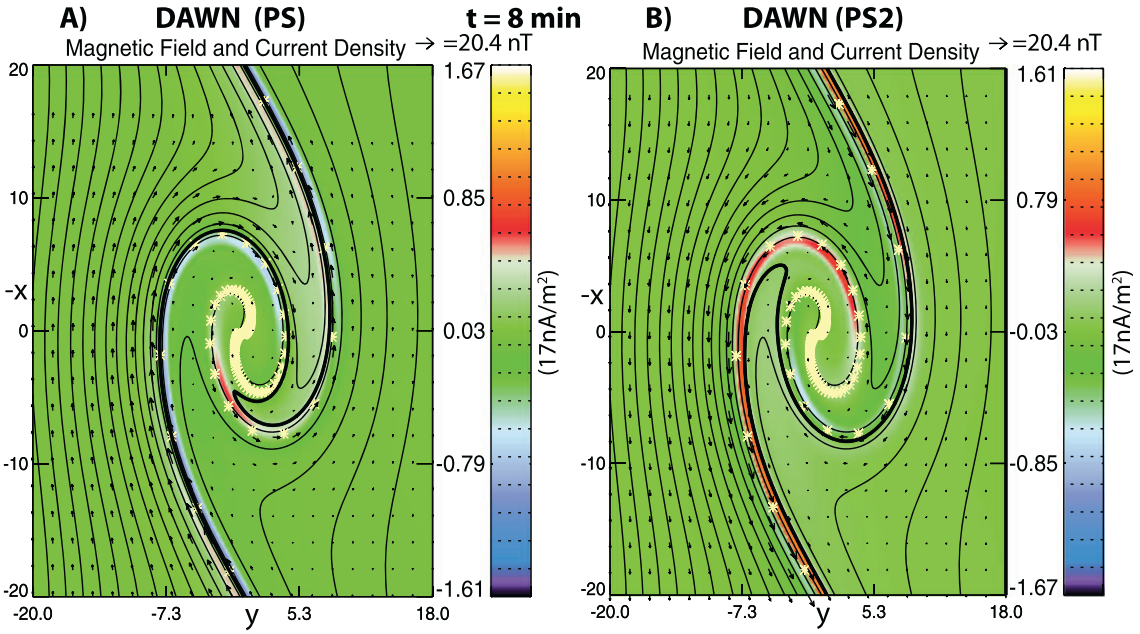

Figure 9. Magnetic field vectors, current density, and magnetic field lines at dawnside flank at t=8 min on the dawn flank for cases (a) 1a and (b) 1b. All length units are normalized to L_0 = 1000 km.

[33] Figure 9 shows the magnetic field (arrows) and plasma current density (background color) for cases 1a (Figure 9a) and 1b (Figure 9b) both on the dawn flank at time t = 8 min. This plot illustrates that while the magnitude of the current is the same for both cases, the direction of the current is not. The IMF orientations, PS or PS2, for the same B_z, determine the direction of the draped tangential magnetic field and thus the direction of the current at the magnetopause (current points to opposite directions in Figures 9a and 9b). Because the magnetic field on the magnetospheric side of the velocity shear layer taken from these global simulations is along the same direction as the magnetosheath field, the Kelvin-Helmholtz growth rate and 2-D reconnection geometry remain the same for both cases. However, for the real magnetosphere, we typically have a case where the tangential component of the magnetospheric field points earthward for $z_{GSM} > 0$ which can result in two different 2-D reconnection geometries for northward IMF. When the horizontal component of the IMF is in the PS (PS2) orientation, the tangential magnetic fields across the velocity shear layer are antiparallel (parallel). This former case has been observed in satellite data, for example, by *Nykyri et al.* [2006] and the latter by *Fairfield et al.* [2000].

[34] Figure 10 shows the growth (maximum velocity perturbation (ln(δv)) in the simulation box perpendicular to the initial current layer) of the KHI at the dawn (solid line) and dusk (dashed line) for 10 different upstream solar wind conditions listed in Table 1. The straight line with constant slope describes the linear growth of the KHI, and when the line saturates, the KHI has reached the nonlinear stage.

[35] For clarity, we have omitted from this plot the cases 1b–1d because they have mirror symmetry such that the dawn flank runs for cases 1a and 1b have exactly the same growth rates as the dusk flank runs for cases 1c and 1d, and similarly, the dusk flank runs for cases 1a and 1b have the same growth rates as the dawn flank runs for 1c and 1d. All of these runs are for northward, Parker spiral IMF or for pure Parker spiral IMF. The SW plasma betas for these 10 runs vary between 0.069 and 5.67 and Alfvén and Magnetosonic Mach numbers from 1.83 to 24.83 and 1.78 to 10.38, respectively, thus presenting a good coverage of SW parameters.

[36] One can see that for all the upstream SW conditions, the growth of the KHI is either slower or fully stabilized on the dusk flank when compared to the dawn flank for the same upstream conditions (the dashed line has always a smaller slope than the solid line of the same color). The fastest growth (greatest slope) occurs for case 4 on the dawn and dusk flanks, respectively, that are both for a 600 km/s solar wind speed. Also, the sum of the MSH and MSP $v_{shear}/\mathbf{V_a} \cdot \mathbf{k}$ ratios (17.48 + 19.11) is largest at the dawn and is the second largest (8.93 + 13.94) at the dusk for case 4.

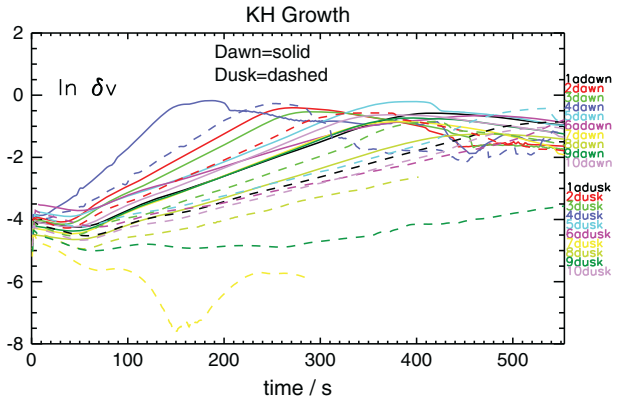

Figure 10. Maximum velocity perturbation (ln(δv)) perpendicular to initial current layer as a function of time for cases 1–10 on the dawnside flank (solid) and on the duskside flank (dashed).

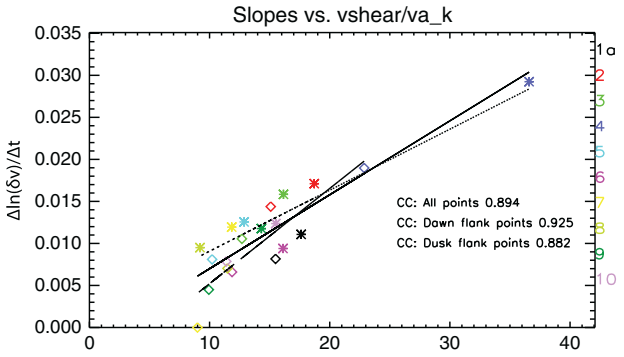

Figure 11. Slopes of the ln(δv) graph (see Figure 10) versus the sum of velocity shear/Alfvén velocity along k vector on magnetospheric and magnetosheath side of the shear flow layer for dawnside (asterisks) and duskside (diamonds) simulations.

[37] Figure 11 shows the slopes of the ln(δv) graph versus the sum of the MSP and MSH ratios between the velocity shear and Alfvén velocity along the k vector (sum of MSP and MSH $v_{\text{shear}}/\mathbf{V_a} \cdot \mathbf{k}$) for all the runs. There is a good correlation (correlation coefficient (cc.) of 0.894) between the slopes and the sum of the MSH and MSP $v_{\text{shear}}/\mathbf{V_a} \cdot \mathbf{k}$ ratio, which is in good agreement with the onset criteria of the KHI (see equations (1) and (2)).

[38] We should also note that in the present global simulations, the velocity shear layer thickness, Δ, is larger than that in the real magnetosphere. For example, for case 1, $\Delta = 3.2\ R_E$. The local simulation growth times are normalized to the local Alfvén speed (which varies between the simulations) travel time over the simulation length unit of $L_0 = 1000$ km. If normalizing the growth times with respect to $\Delta = 3\ L_0$, then each time should be multiplied by factor of 3.

5. Discussion and Conclusions

[39] The presented results indicate that when the IMF is in the Parker spiral (PS) or ortho-Parker spiral (OPS) orientation, the MHD shock physics leads to different properties of the magnetosheath on the dawn flank compared to the dusk flank which can result in asymmetric growth of the Kelvin-Helmholtz instability (KHI) on the two flanks of the magnetosphere. For all the simulation runs presenting a large range of upstream plasma betas and Mach numbers, the KHI growth is observed to be higher on the dawn flank compared to the dusk. For example, for the fastest-growing case (case 4), the nonlinear stage of the instability is reached at 140 s on the dawn flank while it happens about 100 s later on the dusk flank. While for such high-speed solar wind this small difference in KHI growth is not likely to result in strong asymmetries in plasma transport and heating produced by the KHI, the effect can become significant for more typical SW conditions. Namely, the SW conditions for case 6 (magenta color) are calculated from the peak values of the distributions of each plasma and field parameter used for BATS-R-US input obtained from OMNI data during the intervals when the THEMIS spacecraft were in the magnetosheath between 2008 and 2013. For these typical SW conditions during 2008–2013, the nonlinear stage is reached at about 320 s at the dawn and after 600 s at the dusk. The required 600 s KHI growth time at dusk may be too long compared to typical fluctuation time scales in the SW, so the KHI may be stabilized at dusk before it reaches the nonlinear stage.

[40] Because the IMF is statistically most often in PS orientation, this suggests that also in the real magnetosphere, the KHI may favor the dawn flank over the dusk flank. This can result in enhanced plasma transport due to reconnection [*Nykyri and Otto*, 2001], ion diffusion [*Fujimoto and Terasawa*, 1994], and kinetic Alfvén wave (KAW) activity [*Johnson et al.*, 1997] associated with the KHI which may partly explain why *Wing et al.* [2005] observed enhanced densities on the dawnside plasma sheet compared to the duskside. The fact that KHI may statistically favor the dawn flank may also partly explain why the plasma temperatures are higher on the dawnside plasma sheet. Namely, *Nykyri et al.* [2006] observed parallel ion heating during three brief intervals that satisfied good Walén relation and de Hoffman-Teller frame during a KHI event on a PS IMF orientation. Although the fluid signature of reconnection in the Cluster data was consistent with the Walén relations and de Hoffman-Teller frames measured by virtual spacecraft in the simulation box, it remains to be studied whether the observed parallel ion heating is a 2-D or 3-D signature of magnetic reconnection in the KHI vortices. The KAWs can also heat ions perpendicular to the magnetic field [*Johnson et al.*, 1997, 2001], and as mode conversion of the compressional MHD waves can create KAWs [*Lin et al.*, 2010], the enhanced KHI activity on the dawn flank may increase KAW activity resulting in enhanced heating of the plasma sheet ions more on the dawnside.

[41] Additional processes responsible for higher plasma sheet temperatures on the dawn may result from kinetic physics. For the PS orientation, the quasi-parallel shock is statistically on the dawnside magnetosheath, which results in enhanced wave-particle interactions that can heat ions more on the dawn. We are presently carrying out a statistical study using 5+ years of THEMIS data to study the possible magnetosheath temperature asymmetry and correlation with the spatial wave power distribution in the vicinity of ion cyclotron frequency (manuscript in preparation). The seed temperature asymmetry in the magnetosheath plasma may become further enhanced via magnetopause processes such as reconnection, KHI, and KAWs.

[42] The limitation of the present work is the two dimensionality of our KH simulations. For simplicity, we assumed that the k vector lies in the equatorial plane, although in the real magnetosphere, modes can grow with finite k_z, as shown in *Nykyri et al.* [2006]. It therefore may be possible that for some of the cases presented in Figure 10, a faster growth is obtained when the k vector assumes some angle with respect to the initial shear flow layer such that the ratio of the shear flow and Alfvén speed along k vector becomes maximized. In addition, the field line tying into the ionosphere produces a stabilizing effect on the KHI, which is not accounted for in the 2-D system. For these reasons, in order to fully address the asymmetric growth of the KHI arising from different shock geometries at the dawn and dusk flank during PS and OPS orientations, the present study ought to be repeated with high-resolution global MHD simulations that can resolve simultaneously KHI, magnetosphere-ionosphere coupling,

and high-latitude reconnection, as well as include the effects of the dipole tilt.

[43] **Acknowledgments.** K. Nykyri's work is supported by the National Science Foundation grant 0847120. The global simulation results have been provided by the Community Coordinated Modeling Center at Goddard Space Flight Center through their public runs on request system (http://ccmc.gsfc.nasa.gov). In particular, K. Nykyri would like to acknowledge L. Rastaetter for his help to carry out some of the BATS-R-US runs with different numerical solvers for testing purposes. The CCMC is a multiagency partnership between NASA, AFMC, AFOSR, AFRL, AFWA, NOAA, NSF, and ONR. The BATS-R-US model was developed by Tamas Gombosi et al. at the University of Michigan. The original 2.5-D MHD code was developed by Antonius Otto at the University of Alaska Fairbanks.

[44] Philippa Browning thanks the reviewers for their assistance in evaluating this paper.

References

Blanco-Cano, X., N. Omidi, and C. T. Russell (2006), Macrostructure of collisionless bow shocks: 2. ULF waves in the foreshock and magnetosheath, *J. Geophys. Res.*, *111*, A10205, doi:10.1029/2005JA011421.

Chandrasekhar, S. (1961), *Hydrodynamic and Hydromagnetic Stability*, Oxford Univ. Press, New York.

Chen, Q., A. Otto, and L. C. Lee (1997), Tearing instability, Kelvin-Helmholtz instability, and magnetic reconnection, *J. Geophys. Res.*, *102*, 151–161.

Claudepierre, S. G., S. R. Elkington, and M. Wiltberger (2008), Solar wind driving of magnetospheric ULF waves: Pulsations driven by velocity shear at the magnetopause, *J. Geophys. Res.*, *113*, A05218, doi:10.1029/2007JA012890.

Cowee, M. M., D. Winske, and S. P. Gary (2010), Hybrid simulations of plasma transport by Kelvin-Helmholtz instability at the magnetopause: Density variations and magnetic shear, *J. Geophys. Res*, *115*, A06214, doi:10.1029/2009JA015011.

Dimmock, A. P., and K. Nykyri (2013), The statistical mapping of magnetosheath plasma properties based on THEMIS measurements in the magnetosheath interplanetary medium reference frame, *J. Geophys. Res. Space Physics*, doi:10.1002/jgra.50465.

Eastwood, J. P., et al. (2003), On the existence of Alfvén waves in the terrestrial foreshock, *Ann. Geophys.*, *21*, 1457–1465.

Eastwood, J. P., A. Balogh, M. W. Dunlop, and T. S. Horbury (2002), Cluster observations of fast magnetosonic waves in terrestrial foreshock, *Geophys. Res. Lett.*, *29*, 3-1-3-4.

Eastwood, J. P., A. Balogh, C. Mazelle, I. Dandouras, and H. Reme (2004), Oblique propagation of 30 s period fast magnetosonic foreshock waves: A Cluster case study, *Geophys. Res. Lett*, *31*, L04804, doi:10.1029/2003GL018897.

Eastwood, J. P., A. Balogh, E. Lucek, C. Mazelle, and I. Dandouras (2005), Quasi-monochromatic ULF foreshock waves as observed by the four-spacecraft cluster mission: 1. Statistical properties, *J. Geophys. Res*, *110*, A11219, doi:10.1029/2004JA010617.

Fairfield, D. H., R. P. Lepping, E. Hones, S. Bame, and J. Asbridge (1981), Simultaneous measurements of magnetotail dynamics by IMP spacecraft, *J. Geophys. Res.*, *86*, 1396–1414.

Fairfield, D. H., A. Otto, T. Mukai, S. Kokubun, R. P. Lepping, J. T. Steinberg, A. J. Lazarus, and T. Yamamoto (2000), Geotail observations of the Kelvin-Helmholtz instability at the equatorial magnetotail boundary for parallel northward fields, *J. Geophys. Res.*, *105*, 21,159–21,174.

Fairfield, D. H., M. M. Kuznetsova, T. Mukai, T. Nagai, T. I. Gombosi, and A. J. Ridley (2007), Waves on the dusk flank boundary layer during very northward interplanetary magnetic field conditions: Observations and simulation, *J. Geophys. Res.*, *112*, 8206–+, doi:10.1029/2006JA012052.

Fujimoto, M., and T. Terasawa (1991), Ion inertia effect on the Kelvin-Helmholtz instability, *J. Geophys. Res.*, *96*(15), 725.

Fujimoto, M., and T. Terasawa (1994), Anomalous ion mixing within an MHD scale Kelvin-Helmholtz vortex, *J. Geophys. Res.*, *99*, 8601–8614.

Fujimoto, M., and T. Terasawa (1995), Anomalous ion mixing within an MHD scale Kelvin-Helmholtz vortex, 2. Effects of inhomogeneity, *J. Geophys. Res.*, *100*, 12,025–12,034.

Guo, X. C., C. Wang, and Y. Q. Hu (2010), Global MHD simulation of the Kelvin-Helmholtz instability at the magnetopause for northward interplanetary magnetic field, *J. Geophys. Res.*, *115*, A10218, doi:10.1029/2009JA015193.

Hasegawa, H., M. Fujimoto, K. Maezawa, Y. Saito, and T. Mukai (2003), Geotail observations of the dayside outer boundary region: Interplanetary magnetic field control and dawn-dusk asymmetry, *J. Geophys. Res.*, *108*(A4), doi:10.1029/2002JA009667.

Hasegawa, H., M. Fujimoto, Y. Saito, and T. Mukai (2004a), Dense and stagnant ions in the low-latitude boundary region under northward interplanetary magnetic field, *Geophys. Res. Lett.*, *31*, L06802, doi:10.1029/2003GL019120.

Hasegawa, H., M. Fujimoto, T.-D. Phan, H. Reme, A. Balogh, M. W. Dunlop, C. Hashimoto, and R. TanDokoro (2004b), Transport of solar wind into Earth's magnetosphere through rolled-up Kelvin-Helmholtz vortices, *Nature*, *430*, 755–758.

Hasegawa, H., et al. (2009), Kelvin-Helmholtz waves at the Earth's magnetopause: Multiscale development and associated reconnection, *J. Geophys. Res.*, *114*, A12207, doi:10.1029/2009JA014042.

Huba, J. D. (1994), Hall dynamics of the Kelvin-Helmholtz instability, *Phys. Rev. Lett.*, *72*, 2033.

Huba, J. D. (1996), The Kelvin-Helmholtz instability: Finite Larmor radius magnetohydrodynamics, *Geophys. Res. Lett.*, *23*, 2907.

Hwang, K.-J., M. M. Kuznetsova, F. Sahraoui, M. L. Goldstein, E. Lee, and G. K. Parks (2011), Kelvin-Helmholtz waves under southward interplanetary magnetic field, *J. Geophys. Res.*, *116*, A08210, doi:10.1029/2011JA016596.

Johnson, J. R., C. Z. Cheng, and P. Song (1997), Kinetic Alfven waves and plasma transport at the magnetopause, *Geophys. Res. Lett.*, *24*, 1423–1426.

Johnson, J. R., C. Z. Cheng, and P. Song (2001), Signatures of mode conversion and kinetic Alfven waves at the magnetopause, *Geophys. Res. Lett.*, *28*, 227–230.

Keller, K. A., and R. L. Lysak (1999), A two-dimensional simulation of Kelvin-Helmholtz instability with magnetic shear, *J. Geophys. Res.*, *104*(25), 097.

Lavraud, B., M. F. Thomsen, M. G. G. T. Taylor, Y. L. Wang, T. D. Phan, S. J. Schwartz, R. C. Elphic, A. Fazakerley, H. Réme, and A. Balogh (2005), Characteristics of the magnetosheath electron boundary layer under northward interplanetary magnetic field: Implications for high-latitude reconnection, *J. Geophys. Res.*, *110*, A06209, doi:10.1029/2004JA010,808.

Lennartsson, W. (1992), A scenario for solar wind penetration of the Earth's magnetic tail based on ion composition data from the ISEE 1 spacecraft, *J. Geophys. Res.*, *97*, 19,221–19,238.

Li, W., J. Raeder, J. Dorelli, M. Oieroset, and T. D. Phan (2005), Plasma sheet formation during long period of northward IMF, *Geophys. Res. Lett.*, *32*, L12S08, doi:10.1029/2004GL021524.

Li, W. Y., X. C. Guo, and C. Wang (2012), Spatial distribution of Kelvin-Helmholtz instability at low-latitude boundary layer under different solar wind speed conditions, *J. Geophys. Res.*, *117*, A08230, doi:10.1029/2012JA017780.

Lin, Y., J. R. Johnson, and X. Y. Wang (2010), Hybrid simulation of mode conversion at the magnetopause, *J. Geophys. Res.*, *115*, A04208, doi:10.1029/2009JA014524.

Miura, A. (1984), Anomalous transport by magnetohydrodynamic Kelvin-Helmholtz instabilities in the solar wind magnetosphere interaction, *J. Geophys. Res.*, *89*, 801.

Miura, A. (1987), Simulation of the Kelvin-Helmholtz instability at the magnetospheric boundary, *J. Geophys. Res.*, *92*, 3195.

Miura, A. (1990), Kelvin-Helmholtz instability for supersonic shear flow at the magnetospheric boundary, *Geophys. Res. Lett.*, *17*, 749–753.

Miura, A. (1992), Kelvin-Helmholtz instability at the magnetospheric boundary: Dependence on the magnetosheath sonic Mach number, *J. Geophys. Res.*, *97*, 10,655.

Miura, A., and P. L. Pritchett (1982), Nonlocal stability analysis of the MHD Kelvin-Helmholtz instability in a compressible plasma, *J. Geophys. Res.*, *87*, 7431.

Moore, T. W. (2012), Identifying signatures of plasma waves and reconnection associated with Kelvin-Helmholtz activity, MS thesis, Embry-Riddle Aeronautical University, Daytona Beach, Fla.

Nakamura, T. K. M., M. Fujimoto, and A. Otto (2006), Magnetic reconnection induced by weak Kelvin-Helmholtz instability and the formation of the low-latitude boundary layer, *Geophys. Res. Lett.*, *33*, L14106, doi:10.1029/2006GL026318.

Nykyri, K., and A. Otto (2001), Plasma transport at the magnetospheric boundary due to reconnection in Kelvin-Helmholtz vortices, *Geophys. Res. Lett.*, *28*, 3565–3568.

Nykyri, K., and A. Otto (2004), Influence of the Hall term on KH instability and reconnection inside KH vortices, *Ann. Geophys.*, *22*, 935.

Nykyri, K., A. Otto, J. Büchner, B. Nikutowski, W. Baumjohann, L. M. Kistler, and C. Mouikis (2003), Equator-S observations of boundary signatures: FTEs or Kelvin-Helmholtz waves?, in *Earth's Low-Latitude Boundary Layer, Geophys. Monogr. Ser.,* vol. 133, edited by P. T. Newell and T. Onsager, pp. 205–210, AGU, Washington, D. C.

Nykyri, K., A. Otto, B. Lavraud, C. Mouikis, L. Kistler, A. Balogh, and H. Réme (2006), Cluster observations of reconnection due to the Kelvin-Helmholtz instability at the dawn side magnetospheric flank, *Ann. Geophys.*, *24*, 2619–2643.

Oieroset, M., J. Raeder, T. D. Phan, S. Wing, J. P. McFadden, W. Li, M. Fujimoto, H. Rème, and A. Balogh (2005), Global cooling and densification of the plasma sheet during an extended period of purely northward IMF on October 22–24, 2003, *Geophys. Res. Lett.*, *32*, L12S07, doi:10.1029/2004GL021,523.

Onsager, T. G., J. D. Scudder, M. Lockwood, and C. T. Russell (2001), Reconnection at the high-latitude magnetopause during northward interplanetary magnetic field conditions, *J. Geophys. Res.*, *106*(A11), 25,467–25,488.

Otto, A. (1990), 3D resistive MHD computations of magnetospheric physics, *Comput. Phys. Commun.*, *59*, 185–195.

Otto, A., and D. H. Fairfield (2000), Kelvin-Helmholtz instability at the magnetotail boundary: MHD simulation and comparison with Geotail observations, *J. Geophys. Res.*, *105*, 21,175–21,190.

Pu, Z. Y., and M. G. Kivelson (1983), Kelvin-Helmholtz instability at the magnetopause: Solution for compressible plasmas, *J. Geophys. Res.*, *88*, 841.

Russell, C. T., S. M. Petrinec, T. L. Zhang, P. Song, and H. Kawano (1997), The effect of foreshock on the motion of the dayside magnetopause, *Geophys. Res. Lett.*, *24*, 1439–1441., doi:10.1029/97GL01408.

Russell, C. T., G. Le, and S. M. Petrinec (2000), Cusp observations of high- and low-latitude reconnection for northward IMF: An alternate view, *J. Geophys. Res.*, *105*, 5489–5495.

Song, P., and C. T. Russell (1992), Model for the formation of the low-latitude boundary layer for strongly northward interplanetary magnetic field, *J. Geophys. Res.*, *97*, 1411–1420.

Song, P., C. T. Russell, T. I. Gombosi, and D. L. DeZeeuw (2003), A model of the formation of the low-latitude boundary layer for northward IMF by reconnection: A summary and review, in *Earth's Low-Latitude Boundary Layer, Geophys. Monogr. Ser.,* vol. 133, edited by P. T. Newell and T. Onsager, pp. 121–130, AGU, Washington, D. C.

Taylor, M. G. G. T., et al. (2008), The plasma sheet and boundary layers under northward IMF: A multi-point and multi-instrument perspective, *Adv. Space Res.*, *41*, 1619–1629, doi:10.1016/j.asr.2007.10.013.

Terasawa, T., M. Fujimoto, H. Karimabadi, and N. Omidi (1992), Anomalous ion mixing within a Kelvin-Helmholtz vortex in a collisionless plasma, *Phys. Rev. Lett.*, *68*, 2778.

Thomas, V. A. (1995), Three-dimensional kinetic simulation of the Kelvin-Helmholtz instability, *J. Geophys. Res.*, *100*(19), 429.

Thomas, V. A., and D. Winske (1993), Kinetic simulations of the Kelvin-Helmholtz instability at the magnetopause, *J. Geophys. Res.*, *98*, 11,425–11,438.

Tóth, G., et al. (2005), Space Weather Modeling Framework: A new tool for the space science community, *J. Geophys. Res.*, *110*, A12226, doi:10.1029/2005JA011126.

Walsh, B. M., D. G. Sibeck, Y. Wang, and D. H. Fairfield (2012), Dawn-dusk asymmetries in the Earth's magnetosheath, *J. Geophys. Res.*, *117*, A12211, doi:10.1029/2012JA018240.

Wing, S., J. R. Johnson, P. T. Newell, and C.-I. Meng (2005), Dawn-dusk asymmetries, ion spectra, and sources in the northward interplanetary magnetic field plasma sheet, *J. Geophys. Res.*, *110*, A08205, doi:10.1029/2005JA011086.

Yao, Y., C. C. Chaston, K.-H. Glassmeier, and V. Angelopoulos (2011), Electromagnetic waves on ion gyroradii scales across the magnetopause, *Geophys. Res. Lett.*, *38*, L09102, doi:10.1029/2011GL047328.